J|A|C|S
ARTICLES
Published on Web 03/16/2004

Methane-to-Methanol Oxidation by the Hydrated Iron(IV) Oxo Species in Aqueous Solution: A Combined DFT and Car−Parrinello Molecular Dynamics Study

Bernd Ensing*,† Francesco Buda,†,‡ Michiel C. M. Gribnau,§ and Evert Jan Baerends*,†

Contribution from Theoretical Chemistry, Faculty of Sciences, Vrije Universiteit Amsterdam, De Boelelaan 1083, NL-1081 HV Amsterdam, The Netherlands, and Unilever Research Vlaardingen, Postbus 114, Vlaardingen, The Netherlands

Received October 3, 2003; E-mail: ensing@cmm.upenn.edu; baerends@chem.vu.nl

Abstract: Previously, we have shown that the ferryl ion ($[Fe^{IV}O]^{2+}$) is easily produced from Fenton's reagent (i.e., a mixture of Fe^{2+} ions and H_2O_2 in aqueous solution), using DFT and Car−Parrinello MD calculations. To verify that the ferryl ion can indeed act as the active species in oxidation reactions with Fenton's reagent, we study in the present paper the reactivity of the ferryl ion toward an organic substrate, in particular the oxidation of methane to methanol. In the first part of this paper, we perform static DFT calculations on the reaction of CH_4 with the $[(H_2O)_5Fe^{IV}O]^{2+}$ complex in vacuo that show a strong prevalence of the oxygen-rebound mechanism over the methane coordination mechanism. This is in agreement with the static DFT results for methane oxidation by biocatalysts MMO and P450, but not with those for methane oxidation by bare metal-oxo ions, where the methane coordination mechanism prevails. The highest energy barrier in the oxygen-rebound mechanism is only 3 kcal/mol in vacuo, whereas in the methane coordination mechanism the highest barrier is 23 kcal/mol. Overall the oxidation reaction energy is downhill by 47 kcal/mol. We conclude that the ferryl ion can indeed act as the oxidative intermediate in the Fenton oxidation of organic species. In the second part of this paper, we perform a preliminary assessment of solvent effects on the oxidation by the ferryl ion in aqueous solution using the method of constrained (first principles) molecular dynamics. The free energy barrier of the H-abstraction reaction from methane by the ferryl ion (i.e., the first step in the rebound mechanism) in aqueous solution is, with 22 kcal/mol in solution, significantly higher than in vacuo. Given the fact that methane has a relatively strong C−H bond (ca. 10 kcal/mol stronger than the C−H bonds in the more typical Fenton's reagent substrates), we infer that for many organic substrates oxidation with the ferryl ion as an active intermediate may be a perfectly viable route.

I. Introduction

Oxidation of organic compounds catalyzed by transition metal complexes is of great importance in industrial and biological processes. The most efficient oxidation catalysts are enzymes found in nature, and some examples are the chromophore P450, the antitumor drug bleomycin and methane monooxygenase (MMO). MMOs are a group of enzymes with two active iron centers, which are even capable of directly converting methane to methanol, whereas nowadays methanol is commercially produced in a two-step process via synthesis gas, which is thermodynamically less efficient. To improve industrially applied catalysts, study of these enzymes can be very helpful. Oxidations by Fenton's reagent[1,2] (i.e., a mixture of Fe^{2+} and H_2O_2) are particularly interesting because it not only shows several mechanistic similarities with biochemical enzymes but it has also found industrial applications in, for instance, paper bleaching and cleaning of polluted soil. However, the reaction mechanisms within Fenton chemistry, i.e., oxidation reactions initiated by Fenton's reagent, are still not fully understood, despite the intensive research for more than 60 years.

It is generally believed that the active species in Fenton chemistry is the free $OH^{\bullet}$ radical, which is produced by the iron-catalyzed dissociation of hydrogen peroxide, as already proposed in 1932 by Haber and Weiss[3] (reaction eq 1).

$$Fe^{2+} + H_2O_2 \rightarrow Fe^{3+} + OH^- + OH^{\bullet} \quad (1)$$

$$Fe^{2+} + H_2O_2 \rightarrow FeO^{2+} + H_2O \quad (2)$$

According to the most popular alternative, the active intermediate is a high-valent iron oxo species, the ferryl ion, which was actually already suggested in 1930 by Bray and Gorin[4] (reaction eq 2). Due to the extremely short lifetimes of the proposed active intermediates, which makes direct detection experimentally very difficult, the controversy remains. The

† Vrije Universiteit Amsterdam.
‡ Present address: Leiden Institute of Chemistry, Leiden University, P.O. Box 9502, 2300 RA, Leiden, The Netherlands.
§ Unilever Research Vlaardingen.

(1) Fenton, H. J. H. *Chem. News* **1876**, 190.
(2) Fenton, H. J. H. *J. Chem. Soc.* **1894**, *65*, 899.
(3) Haber, F.; Weiss, J. *Proc. R. Soc. London* **1934**, *147*, 332.
(4) Bray, W. C.; Gorin, M. H. *J. Am. Chem. Soc.* **1932**, *54*, 2124.

elucidation of the mechanism is further complicated by its complex dependence on reaction conditions such as the ligation of the metal, the solvent, the pH, and the organic substrate.

We have recently performed static density functional theory (DFT) calculations on water-ligated iron hydrogen peroxide complexes in vacuo as well as ab initio (DFT) molecular dynamics (AIMD) simulations on Fenton's reagent in aqueous solution, without an organic substrate.[5−9] Our studies show that the ferryl ion is easily formed from hydrogen peroxide coordinated to pentaaqua iron(II) and, from the energetic point of view, much more likely than the formation of free $OH^{\bullet}$ radicals, thus favoring Bray and Gorin's proposal (reaction eq 2). However, to definitively accept the ferryl ion as the active species in aqueous Fenton chemistry, we need to investigate whether the ferryl ion is indeed capable of oxidizing organic substrates. This is the main goal of the present study.

For the organic substrate, we have chosen methane as our model system, which commends itself for a number of reasons. First, the conversion of methane to methanol is commercially very interesting, as mentioned before. Second, methane is a simple and small system, which should limit the chemical complexity and also the computational requirements. Third, since the C−H dissociation energies of alkanes range from 103 kcal/mol (calculated at the DFT-BP+ZPE level of theory) for methane to about 90 kcal/mol for tertiary positions, oxidation of other alkanes by the ferryl ion should proceed more readily. Last, C−H bond activation of methane by transition metal complexes has already been investigated extensively, which makes it possible to compare the reactivity of the water-ligated iron oxo species to other iron-oxo moieties such as the previously mentioned enzymes. In practice, methane is not a Fenton's reagent substrate in aqueous solution due to its very low solubility in water.

The bare FeO^+ ion has been shown to oxidize methane to methanol in the gas phase, under ion-cyclotron resonance conditions,[10,11] which has led to a number of theoretical investigations of oxidation reactions by FeO^+ and other bare metal oxo species.[12−18] Bare iron-oxo species were also believed to model the enzyme oxidations by cytochrome P450[17] and MMO.[12−14] For the methane-to-methanol oxidation by FeO^{n+}, $n = 0, 1, 2$, Yoshizawa et al. found that a concerted reaction mechanism, via a four-centered transition state (with methane coordinated to iron), is energetically more favorable than a direct H-abstraction by the oxo ligand. Second, FeO^{2+} is much more effective for C−H bond cleavage in this *methane coordination mechanism* than FeO^+ and FeO.[12] Also, MnO^+, which is isoelectronic to FeO^{2+}, is most effective in C−H bond activation, compared to FeO^+ and CoO^+.[13,19] Shaik et al. have proposed low-energy reaction paths, via a double crossing of the high-spin and low-spin energy surfaces, the so-called two-state reactivity.[17,18,20] However, in contrast to FeO and FeO^+, the spin inversion is unlikely to play a role in the FeO^{2+} case. Only the quintet state plays a role in the C−H activation by the aqueous ferryl ion.[12]

The active states of the bioorganic molecules MMO[21−23] and cytochrome P450,[24,25] capable of hydroxylating and oxidizing organic substrates, also involve an $Fe^{IV}O$ intermediate. The latest theoretical (DFT) studies on methane-to-methanol oxidation by MMO[26−33] and P450[34,35] confirm the consensus *oxygen-rebound mechanism* for these systems. The rate-limiting step is the methane H-abstraction, via a linear (Fe)O···H···C complex, forming a $^{\bullet}CH_3$ radical, which can rearrange to form the alcohol in the rebound step. The oxygen-rebound mechanism is supported by the high measured[36−38] and calculated[34,39] kinetic isotope effects. However, ultrafast radical clock experiments, timing the rate of the rebound step, have measured extremely short intermediate lifetimes, casting doubt on the presence of free radicals, which occur in a rebound mechanism.[40,41] Ogliaro et al. explained the fast radical clock results for the P450 system with the aforementioned two-state reactivity.[35] For MMO, the radical clock experiments were explained by Siegbahn by an electron transfer of the substrate to the metal complex, forming a cation instead of a free radical.[27]

We start with a summary of the methodological details in section II. Then, in section III, we focus on the reaction energy profiles for the oxidation of methane to methanol by the water-ligated iron(IV) oxo species in vacuo following the two mechanisms proposed in the literature. (A third mechanism, the so-called oxene insertion, is now generally believed to be unlikely, as it is characterized by very high energy barriers.[18])

(5) Buda, F.; Ensing, B.; Gribnau, M. C. M.; Baerends, E. J. *Chem. Eur. J.* **2001**, *7*, 2775.
(6) Ensing, B.; Buda, F.; Blöchl, P. E.; Baerends, E. J. *Angew. Chem., Int. Ed.* **2001**, *40*, 2893.
(7) Ensing, B.; Buda, F.; Blöchl, P. E.; Baerends, E. J. *Phys. Chem. Chem. Phys.* **2002**, *4*, 3619.
(8) Ensing, B.; Baerends, E. J. *J. Phys. Chem. A.* **2002**, *106*, 7902.
(9) Buda, F.; Ensing, B.; Gribnau, M. C. M.; Baerends, E. J. *Chem. Eur. J.* **2003**, *9*, 3436.
(10) Schröder, D.; Schwarz, H. *Angew. Chem., Int. Ed.* **1990**, *29*, 1433.
(11) Schröder, D.; Schwarz, H.; Clemmer, D. E.; Chen, Y.; Armentrout, P. B.; Baranov, V. I.; Bohme, D. K. *Int. J. Mass Spectrom.* **1997**, *161*, 175.
(12) Yoshizawa, K.; Shiota, Y.; Yamabe, T. *Organometallics* **1998**, *17*, 2825.
(13) Yoshizawa, K.; Shiota, Y.; Yamabe, T. *J. Am. Chem. Soc.* **1998**, *120*, 564.
(14) Yoshizawa, K.; Shiota, Y.; Yamabe, T. *J. Chem. Phys.* **1999**, *111*, 538.
(15) Yoshizawa, K.; Shiota, Y.; Kagawa, Y.; Yamabe, T. *J. Phys. Chem. A* **2000**, *104*, 2552.
(16) Schröder, D.; Schwarz, H.; Shaik, S. *Struct. Bond.* **2000**, *97*, 92.
(17) Shaik, S.; Filatov, M.; Schröder, D.; Schwarz, H. *Chem. Eur. J.* **1998**, *4*, 193.
(18) Filatov, M.; Shaik, S. *J. Phys. Chem. A* **1998**, *102*, 3835.
(19) Ryan, M. F.; Fiedler, A.; Schröder, D.; Schwarz, H. *J. Am. Chem. Soc.* **1995**, *117*, 2033.
(20) Fiedler, A.; Schröder, D.; Shaik, S.; Schwarz, H. *J. Am. Chem. Soc.* **1994**, *116*, 10734.
(21) Feig, A. L.; Lippard, S. J. *Chem. Rev.* **1994**, *94*, 759.
(22) Waller, B. J.; Lipscomb, J. D. *Chem. Rev.* **1996**, *96*, 2625.
(23) Solomon, E. I.; Brunold, T. C.; Davis, M. I.; Kemsley, J. N.; Lee, S.-K.; Lehnert, N.; Neese, F.; Skulan, A. J.; Yang, Y.-S.; Zhou, J. *Chem. Rev.* **2000**, *100*, 235.
(24) Ortiz de Montellano, P. R.; *Cytochrome P450: Structure, Mechanism, and Biochemistry*; Plenum: New York, 1995.
(25) Sono, M.; Roach, M. P.; Coulter, E. D.; Dawson, J. H. *Chem. Rev.* **1996**, *96*, 2841.
(26) Siegbahn, P. E. M.; Crabtree, R. H. *J. Am. Chem. Soc.* **1997**, *119*, 3103.
(27) Siegbahn, P. E. M. *J. Biol. Inorg. Chem.* **2001**, *6*, 27.
(28) Basch, H.; Mogi, K.; Musaev, D. G.; Morokuma, K. *J. Am. Chem. Soc.* **1999**, *121*, 7249.
(29) Basch, H.; Mogi, K.; Musaev, D. G.; Morokuma, K. *J. Phys. Chem. A* **2001**, *105*, 3615.
(30) Torrent, M.; Musaev, D. G.; Basch, H.; Morokuma, K. *J. Comput. Chem.* **2002**, *23*, 59.
(31) Dunietz, B. D.; Beachy, M. D.; Cao, Y.; Whittington, D. A.; Lippard, S. J.; Friesner, R. A. *J. Am. Chem. Soc.* **2000**, *122*, 2828.
(32) Gherman, B. F.; Dunietz, B. D.; Whittington, D. A.; Lippard, S. J.; Friesner, R. A. *J. Am. Chem. Soc.* **2001**, *123*, 3836.
(33) Guallar, V.; Gherman, B. F.; Miller, W. H.; Lippard, S. J.; Friesner, R. A. *J. Am. Chem. Soc.* **2002**, *124*, 3377.
(34) Ogliaro, F.; Filatov, M.; Shaik, S. *Eur. J. Inorg. Chem.* **2000**, 2455.
(35) Ogliaro, F.; Harris, N.; Cohen, S.; Filatov, M.; de Visser, S. P.; Shaik, S. *J. Am. Chem. Soc.* **2000**, *122*, 8977.
(36) Nesheim, J. C.; Lipscomb, J. D. *Biochemistry* **1996**, *35*, 10240.
(37) Lipscomb, J. D.; Que, L., Jr. *J. Biol. Inorg. Chem.* **1998**, *3*, 331.
(38) Brazeau, B. J. Waller, B. J.; Lipscomb, J. D. *J. Am. Chem. Soc.* **2001**, *123*, 1042.
(39) Yoshizawa, K.; Kagawa, Y.; Shiota, Y. *J. Phys. Chem. B* **2000**, *104*, 12365.
(40) Toy, P. H.; Newcomb, M.; Hollenberg, P. F. *J. Am. Chem. Soc.* **1998**, *120*, 7719.
(41) Newcomb, M.; Shen, R.; Choi, S. Y.; Toy, P. H.; Hollenberg, P. F.; Vaz, A. D. N.; Coon, M. J. *J. Am. Chem. Soc.* **2000**, *122*, 2677.

Table 1. Bond Dissociation Energies and Rearrangement Energies in kcal/mol for Isolated ("Gas Phase") Complexes, Calculated with the Amsterdam Density Functional Program (ADF) and the CP-PAW Program Using the Becke−Perdew Exchange Correlation Functional]

	gas-phase reaction	CP-PAW	ADF	$\Delta\Delta E$
A	$[(H_2O)_6Fe^{II}]^{2+} \rightarrow [(H_2O)_5Fe^{II}]^{2+} + H_2O$	21.7	22.1	−0.4
B	$[(H_2O)_6Fe^{II}]^{2+} \rightarrow [(H_2O)_5Fe^{II}]^{2+} - H_2O$	−2.3	−3.5	1.2
C	$[Fe^{II}(H_2O)_5]^{2+} + H_2O_2 \rightarrow [Fe^{III}(H_2O)_5OH]^{2+} + OH^{\bullet}$	−8.4	−2.1	−6.3
D	$[Fe^{III}(H_2O)_5OH]^{2+} + OH^{\bullet} \rightarrow [Fe^{IV}(H_2O)_5O]^{2+} + H_2O$	−30.8	−28.7	−2.1

The results for the methane coordination mechanism are presented in section III-A, and next we discuss the results for the oxygen-rebound (radical) mechanism in section III-B. The in vacuo results clearly establish the oxygen rebound mechanism as the favored one, with only a barrier of 3 kcal/mol, and prove the viability of Fenton oxidation via the FeO^{2+} intermediate. In the remainder of the paper (section IV), a first investigation is made of the (usually neglected) role of the environment of the reactants on the thermodynamics of the C−H activation. Traditionally, Fenton chemistry takes place in aqueous solution. We have therefore computed the free energy profile for the methane hydroxylation by the ferryl ion (according to the oxygen-rebound mechanism) in aqueous solution, using constrained ab initio molecular dynamics. It is clear that water is not the natural solvent for methane, so we have to treat these results with caution when making inferences for typical organic substrates for the Fenton reaction, which are water soluble and have less strong C−H bonds; see the discussion in section IV-B. The conclusions are summarized in section V.

II. Methods

In view of the strongly spin-polarized nature of Fe in the complexes, all electronic structure calculations were performed using the *unrestricted* density functional theory (DFT) method (e.g., see ref 42). Note that the lowest state of the iron(IV) oxo complex is the high-spin state ($S = 2$),[5] and this overall spin state is actually preserved during all the further transformations that are considered in this paper. The spin states will therefore only be referred to if they are not completely evident from this information. We used the Becke-88 gradient-corrected exchange functional[43] and the Perdew-86 gradient-corrected correlation functional.[44] For the first part of the paper on the molecular structures in vacuo, we used the Slater-type orbital-based ADF package[45] for the calculation of energies, frequencies, and optimizations of geometries. The Kohn−Sham orbitals were expanded in a large, even-tempered, all-electron, Slater-type basis set containing 4s, 2p, and 1d functions for hydrogen; 6s, 4p, 2d, and 1f functions for carbon and oxygen; and 11s, 7p, 5d, and 1f functions for iron.[46] Finite-temperature reaction enthalpies at $T = 300$ K and the entropies were estimated using

$$\Delta H^{300K} = \Delta E_0 + \Delta E_{ZPE} + \Delta E_{int}^{300K} \quad (3)$$

$$\Delta E_{int}^{300K} = \Delta E_T{}^{v} + \Delta E^{t} + \Delta E^{r} \quad (4)$$

$$\Delta S = R \ln(Q^{t} Q^{r} Q^{v}) \quad (5)$$

with E_0 being the sum of the electronic energy in a static nuclear field (Born−Oppenheimer approximation) and the nuclear electrostatic repulsion. The zero-point vibrational energy E_{ZPE} and the temperature-dependent vibrational energy $E_T{}^{v}$ were calculated from the unscaled DFT-BP frequencies, within the harmonic approximation. The change in translational energy ΔE^{t} and rotational energy ΔE^{r} were obtained using the ideal gas law, associating $1/2\ k_B T$ to each degree of freedom. The partition function Q is the product of translational, rotational, and vibrational contributions (e.g., see Chapter 20 in ref 47).

For the second part of the paper on the ab initio (DFT) molecular dynamics calculations of the systems including the solvent environment, we used the Car−Parrinello (CP) method[48] as implemented in the CP−PAW code developed by Blöchl.[49] The one-electron valence wave functions were expanded in an augmented plane wave basis up to a kinetic energy cutoff of 30 Ry. The frozen core approximation was applied for the 1s electrons of O and up to 3p for Fe. For the augmentation for H and O, one projector function per angular momentum quantum number was used for s- and p-angular momenta. For Fe, one projector function was used for s- and p-, and two were used for d-angular momenta. The characteristic feature of the Car−Parrinello approach is that the electronic wave function, i.e., the coefficients of the plane wave basis set expansion, are dynamically optimized to be consistent with the changing positions of the atomic nuclei. The mass for the wave function coefficient dynamics was $\mu_e = 1000$ au, which limits the MD time step to $\delta t = 0.19$ fs.

The advantage of PAW over the more commonly used pseudopotential approach is that transferability problems should be largely avoided. However, as with all methods in which the core is represented approximately, there will be some loss of accuracy. Extensive tests are therefore required, and we have previously shown that bond energies and geometries of small molecules and complexes computed with CP−PAW agree very well with highly accurate all-electron DFT results obtained with the ADF program.[50] However, we have in the course of the present work noted that reaction energies of chemical reactions involving a change in the formal oxidation state of iron sometimes exhibit relatively large (several kcal/mol) discrepancies with accurate (large basis set, all-electron) ADF calculations. Table 1 shows four reaction energies of gas-phase reactions involving simple water-ligated iron complexes, calculated with CP−PAW and ADF.

Reactions A and B show the typical small differences in the order of 1 kcal/mol due to the differences in basis set and the frozen core approximation used with PAW. However, reactions C and D, which involve a change in the iron oxidation state, show larger discrepancies, up to 6.3 kcal/mol for the reaction in which iron(II) is oxidized to iron(III). The error does not seem to be due to the plane-wave cutoff of 30 Ry (it is not reduced when going to 50 Ry) and can be attributed to the partial waves for the inner region of the valence electrons and the projector functions used in the PAW calculations. Also in this work, we simulate a reaction involving a changing iron oxidation state (from iron(IV) to iron(III)) in aqueous solution. We will therefore only discuss the solvent effects on this reaction by comparing the results with the same reaction in vacuo rather than attempting to compute the reaction rate for this reaction in aqueous solution.

III. Gas-Phase Calculations

A. Methane Coordination Mechanism. Figure 1 shows the energy profile and the complex geometries along the reaction

(42) Parr, R. G.; Yang, W. *Density-Functional Theory of Atoms and Molecules*; Oxford University: New York, 1989.
(43) Becke, A. D. *J. Chem. Phys.* **1992**, *96*, 2155.
(44) Perdew, J. P. *Phys. Rev. B* **1986**, *33*, 8822.
(45) Baerends, E. J.; Ellis, D. E.; Ros, P. *Chem. Phys.* **1973**, *2*, 41.
(46) Chong, D. P. Private communication on high-quality even-tempered all-electron STO basis set.
(47) Atkins, P. W. *Physical Chemistry*; Oxford University Press: New York, 1990.
(48) Car, R.; Parrinello, M. *Phys. Rev. Lett.* **1985**, *55*, 2471.
(49) Blöchl, P. E. *Phys. Rev. B* **1994**, *50*, 17953.
(50) Ensing, B.; Meijer, E. J.; Blöchl, P. E.; Baerends, E. J. *J. Phys. Chem. A* **2001**, *105*, 3300.

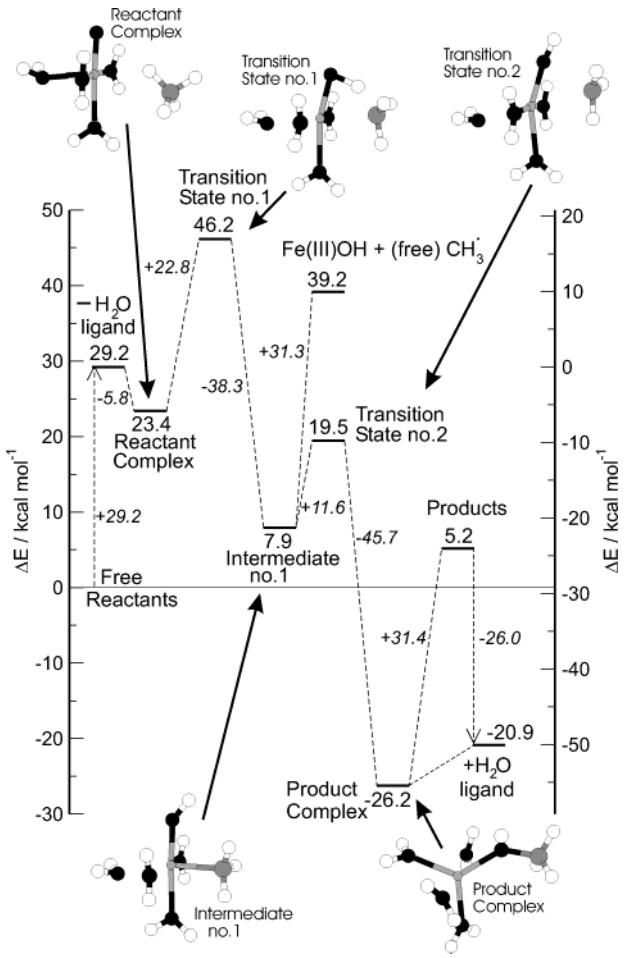

Figure 1. Geometries and energy profile (in kcal/mol) of the intermediate steps along the methane coordination mechanism of the methane-to-methanol oxidation by the pentaaqua iron(IV) oxo species. The energy of the separated reactants is the off set for the left-hand-side energy axis. The energy axis on the right-hand-side serves to indicate the energy changes with respect to the separate tetraaqua iron(IV) oxo complex and methane molecule, i.e., after creating a vacant coordination site.

coordinate for the reaction between tetraaqua iron(IV) oxo and methane, following the methane coordination mechanism. Starting from the octahedrally coordinated pentaaqua iron(IV) oxo complex, the oxidation reaction is thus preceded by the opening of a coordination site for the methane. The required expulsion of a water ligand is endothermic by 29.2 kcal/mol in vacuo. For comparison with the rebound mechanism hereafter, which has the pentaaqua iron(IV) oxo complex as a starting species, we will use also here the sum of the energies of the optimized pentaaqua iron(IV) oxo complex and the optimized methane molecule as the zero of the energy scale (shown on the left-hand-side vertical axis in Figure 1). As the solvent-mediated leaving of the water ligand is believed to be much less endothermic in aqueous solution, we have added a second axis on the right-hand-side to show the energy changes with respect to the separated tetraaqua iron(IV) oxo ion and methane reactants. The initial step of the reaction with methane is the coordination of methane at the vacant coordination site of the metal center, forming a weekly bound reactant complex. The interaction energy is less than 6 kcal/mol. The transformation of the reactant complex into the product complex of methanol bound to tetraaqua iron(II) occurs in two steps. In the first step, a hydrogen is abstracted from the weakly bound methane by the oxo-ligand, forming a hydroxo ligand and a CH_3 ligand, making iron formally Fe^{IV} (see intermediate no. 1 in Figure 1). This step is exothermic by 15.5 kcal/mol but has a significant barrier of 22.8 kcal/mol with respect to the reactant complex, associated with a strained four-membered ring in the transition state. In the second step, the CH_3 group is transferred from the metal center to the oxygen of the hydroxo ligand, forming a bound methanol group. The oxidation state of iron is simultaneously lowered from Fe^{IV} to Fe^{II}, as both ligands (i.e., formally OH^- and CH_3^-) revert formally to $OH^\bullet$ and $CH_3^\bullet$ to form an electron pair bond in CH_3OH, i.e., donate an electron to the metal d-manifold. The energy barrier for the, again exothermic, second step is not very high: 11.6 kcal/mol. This second barrier is much lower than the energy required to, alternatively, form a free $CH_3^\bullet$ radical and the iron(III) hydroxo complex from intermediate no. 1 (+31.3 kcal/mol).

The bonding of the methanol to $Fe^{II}(H_2O)_4$ is found to be 31.4 kcal/mol strong. The final separation in aqueous solution can, however, be expected to be almost thermoneutral (ΔE = 5.4 kcal/mol, neglecting solvent effects) if it is accompanied by the coordination of a solvent water to the vacant coordination site of the 5-fold-coordinated product complex, i.e.:

$$Fe^{II}(H_2O)_4(CH_3OH) + H_2O \rightarrow Fe^{II}(H_2O)_5(CH_3OH) \qquad \Delta E = -20.3 \text{ kcal/mol}$$

$$Fe^{II}(H_2O)_5(CH_3OH) \rightarrow Fe^{II}(H_2O)_5 + CH_3OH \qquad \Delta E = +25.7 \text{ kcal/mol}$$

(methanol is more strongly bonded to tetraaqua iron(II) than to pentaaqua iron(II) by 31.4 − 25.7 = 5.7 kcal/mol).

Compared to the methane-to-methanol oxidation by bare metal-oxo species,[12−18] for which the methane coordination mechanism was found to be the most likely mechanism, there are a number of differences. In the reactant complexes of methane coordinated to bare FeO, FeO^+, and FeO^{2+}, the binding of methane is η^2- or η^3-type, with Fe−C distances as short as 2.32, 2.36, and 2.07 Å, respectively.[12] The interaction energy between CH_4 and FeO^{2+} was found to be extremely high, namely, 70.3 kcal/mol, compared to 22.8 and 5.7 kcal/mol, for coordination of methane to the high-spin FeO^+ and FeO molecules, respectively. The interaction energy with the MnO^+ ion (which is isoelectronic with FeO^{2+}) is only 16.2 kcal/mol.[13] Instead, we find for our water-ligated complexes only a weak interaction between methane and the iron(IV) complex (5.8 kcal/mol), with methane bonded to the metal via a single hydrogen, the Fe−H bond distance being 2.17 Å, and the Fe−C distance being 3.02 Å. The relevant geometrical parameters, as well as Mulliken charges q and spin populations s are compiled in Table 2 for the structures shown in Figure 1. The Mulliken charge on iron of qFe = 1.22 is relatively high compared to, e.g., the 5-fold-coordinated $[Fe^{IV}(OH)_4(H_2O)]\cdot H_2O$ complex (qFe = 0.85[26]), due to the total +2 charge of our systems, and hardly changes after forming the reactant complex with methane. Also, the different basis sets used in our work and in that in the literature can give rise to differences in the Mulliken charges, so these comparisons are to be regarded with reservation. The spin-density on iron(IV) of sFe = 3.10, on the other hand, agrees very well that of other iron(IV) complexes such as the tetrahydroxo complex (sFe = 3.10[26]) and in MMO models (sFe

Table 2. Relevant Bond Lengths (in Å) and Angles as Well as Mulliken Charges and Spin Populations for the Reaction Intermediates in the Methane Coordination Mechanism of the Methane-to-Methanol Oxidation by the Tetraaqua Iron(IV) Oxo Species

	free reactants	reactant complex	transition state 1	intermediate 1	transition state 2	product complex	free products
*R*FeO	1.62	1.61	1.73	1.74	1.79	2.03	
*R*OH		2.51	1.13	0.98	0.97	0.97	0.97
*R*FeC		3.02	2.20	2.06	2.46	3.18	
*R*OC		3.62	2.34	2.70	2.18	1.48	1.43
*R*CH	1.10	1.12	1.30	2.90	2.40	2.02	1.96
∠OFeC		98°	72°	90°	59°	21°	
*q*Fe	1.22	1.24	1.43	1.40	1.32	1.25	1.28
*q*O	−0.16	−0.20	−0.25	−0.21	−0.30	−0.08	−0.09
*q*C	0.30	0.41	0.19	0.20	0.41	0.29	0.22
*q*H	−0.08	−0.11	0.03	0.08	0.08	0.06	0.07
*s*Fe	3.10	3.07	3.68	3.74	3.87	3.82	3.84
*s*O	0.73	0.72	0.28	0.37	0.26	0.04	0.00
*s*C	0.00	0.04	−0.19	−0.32	−0.31	0.00	0.00
*s*H	0.00	0.01	0.05	0.02	0.01	0.00	0.00

$= 3.11-3.55$[27−29]). The rest of the spin-density (the integrated spin-density is 4) is mainly located on the oxo ligand. The geometries of transition state no. 1 (TS1) and the hydroxo intermediate agree qualitatively with the ones found for this first step for the bare $[FeO-HCH_3]^{2+}$.[12] Quantitatively, the bond lengths differ on the order of 0.1 Å, with notably shorter Fe−O bond lengths of 1.614 and 1.675 Å for the TS1 and intermediate, respectively, in the case of the bare $[FeO-HCH_3]^{2+}$ (while in the water-ligated complexes we find bond lengths of 1.73 and 1.74 Å) and a larger O−H bond distance of 1.443 Å for the transition state (we find 1.13 Å). The energetics are again very different. For the bare $[FeO-HCH_3]^{2+}$ first step, the barrier is only 4.9 kcal/mol (here, 22.8 kcal/mol), whereas the overall transformation energy equals −52.0 kcal/mol (we find −15.5 kcal/mol). The $[MnO-CH_3]^+$ profile shows only slightly better comparison, with a barrier of 9.4 and −36.1 kcal/mol overall.

The second step, the formation of the methanol, which we find to be exothermic by 34.1 kcal/mol with a moderate barrier of 11.6 kcal/mol, was found to be energetically unfavorable for the bare $[FeOH-CH_3]^{2+}$ case and was not further discussed.[12] Also with manganese (i.e., bare $[MnOH-CH_3]^{2+}$), this step is not exothermic (by 0.2 kcal/mol) and has a very high barrier, equal to 35.9 kcal/mol.[13]

We conclude that the oxidation of methane to methanol by the tetraaqua iron(IV) oxo species is exothermic in vacuo following the methane coordination pathway, with a highest barrier for the hydroxylation step of 22.8 kcal/mol with respect to the reactant complex state. If one were to start from pentaaqua iron(IV) oxo (as in aqueous solution), the first step is the water−methane ligand exchange reaction, which in vacuo is endothermic by 23.4 kcal/mol. The reaction energy profile shows large differences with that of methane oxidation by a bare FeO^{2+} ion, which casts doubt on the use of bare transition metal-oxo species as models for ligated transition metal oxo moieties such as occur in enzymes and generally in solution.

B. Rebound Mechanism. In this section, we present the results for the methane-to-methanol oxidation by the water-ligated iron(IV) oxo species, following the oxygen-rebound mechanism. This mechanism also consists of two steps: first, the hydrogen abstraction from methane by the iron(IV) oxo species, producing iron(III) hydroxo and a $^{\bullet}CH_3$ radical, and second, the collapse of the $^{\bullet}CH_3$ radical onto the iron(III) hydroxo oxygen, forming $Fe(II)CH_3OH$. Figure 2 shows the energy profile for these reaction steps along with the intermediate complex structures. For this mechanism, we have also

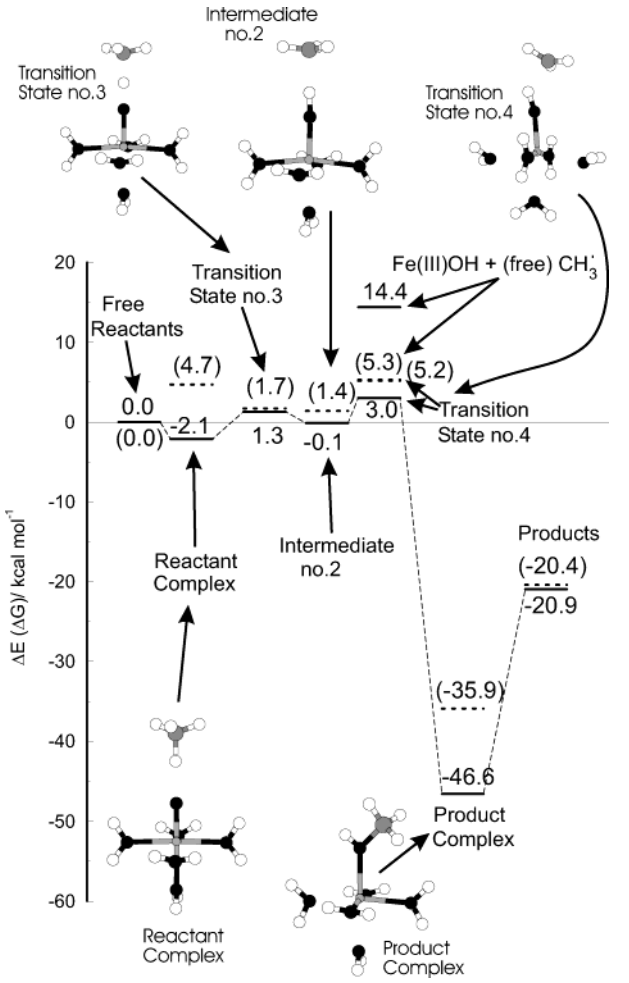

Figure 2. Geometries and energy profile (in kcal/mol) of the intermediate steps along the oxygen-rebound mechanism of the methane-to-methanol oxidation by the pentaaqua iron(IV) oxo species. The energy of the separated reactants is set to zero. The free energies are indicated by the dotted levels and the numbers between parenthesis.

computed the zero-point energy corrections, the temperature-dependent enthalpy corrections for a temperature of $T = 300$ K, and the entropy term $-T\Delta S$ (see Table 3), the sum of which is added to the internal energy to give the free energy, indicated in Figure 2 between parentheses.

The interaction between the methane substrate and the iron(IV) oxo complex is again very weak in the reactant complex, equal to −2 kcal/mol. The first reaction step, the transfer of a

Table 3. DFT Energies (kcal/mol) for the Intermediates in the Oxygen-Rebound Mechanism of the Methane-to-Methanol Oxidation by the Pentaaqua Iron(IV) Oxo Species (Proposed Active Species in Fenton's Reagent), Compared to Biochemical Methane Oxidations by MMO and P450[a]

	reactant complex	transition state 3	intermediate 2	free radical	transition state 4	product complex	free products
Fenton[b]	−2.1	1.3	−0.1	14.4	3.0	−46.6	−20.9
MMO[c]	2.3	13.8	2.8		7.6	−47.7	
MMO[d]	−1.5	23.2	11.3	23.7	20.6	−41.8	−34.3
P450[e]	−1.0	26.7	23.6		29.1	−36.9	
ΔZPE[b]	−0.8	−4.9	−3.3	−3.9	−3.5	1.8	0.1
ΔE_{int}^{300K}[b]	0.4	−4.4	−1.7	−1.8	−2.1	4.2	−1.3
$-T\Delta S$[b]	7.2	9.7	6.6	−3.4	7.8	4.6	1.7

[a] Bottom three rows show the zero-point energy correction, temperature-dependent corrections, and the entropy term [b] Our work. [c] P. E. M. Siegbahn, DFT-B3LYP + PCM, MMO compound Q model: $(HCOO)_2-(C_3N_2H_4)Fe(\mu\text{-}O)_2(\eta^2\text{-}HCOO)Fe(C_3N_2H_4)(HCOO)(H_2O)$, ref 27. [d] Basch et al., DFT-B3LYP, MMO compound Q model: *cis*-$(H_2O)(NH_2)Fe(\mu\text{-}O)_2(\eta^2\text{-}HCOO)_2Fe(NH_2)(H_2O)$, ref 29. [e] Ogliaro et al., DFT-B3LYP, high-spin P450 compound I model: $FeO(C_{20}N_4H_{12})(HS)$, ref 35.

Table 4. Relevant Bond Lengths (in Å) and Angles as Well as Mulliken Charges and Spin Populations for the Reaction Intermediates in the Oxygen-Rebound Mechanism of the Methane-to-Methanol Oxidation by the Pentaaqua Iron(IV) Oxo Species

	free reactants	reactant complex	transition state 3	intermediate 2	free radical	transition state 4	product complex	free products
*R*FeO	1.61	1.63	1.72	1.77	1.77	1.79	2.09	
*R*OC		2.91	2.55	2.78		2.50	1.47	
*R*OH		1.76	1.20	1.03	0.98	1.01	0.97	1.43
*R*CH	1.10	1.15	1.34	1.76		1.70	1.99	0.97
∠HOC		1°	0°	1°		30°	108°	108°
∠FeOH		179°	176°	155°	179°	151°	120°	
*q*Fe	1.35	1.36	1.46	1.43	1.49	1.43	1.30	1.33
*q*O	−0.20	−0.30	−0.48	−0.36	−0.25	−0.37	−0.08	−0.09
*q*C	0.30	0.34	0.34	0.30	0.00	0.33	0.30	0.22
qCH_3	0.08	0.13	0.32	0.32	0.00	0.34	0.21	0.02
*q*H	−0.08	−0.11	0.04	−0.03	0.07	−0.02	0.05	0.07
*s*Fe	3.14	3.40	3.97	4.11	4.20	4.08	3.83	3.85
*s*O	0.69	0.59	0.38	0.40	0.52	0.35	0.04	0.00
*s*C	0.00	−0.10	−0.50	−0.75	1.08	−0.65	0.00	0.00
*s*H	0.00	−0.04	−0.03	−0.01	0.03	−0.01	0.00	0.00

CH_4 hydrogen from methane to the oxo ligand, forming an Fe(III)OH complex with a bound $^{\bullet}CH_3$ radical (intermediate no. 2 in Figure 2), is surprisingly easy. The reaction energy with respect to the reactant complex is +2.0 kcal/mol, and the barrier is only 3.4 kcal/mol (1.3 kcal/mol with respect to the free reactants). In contrast to H-abstraction from an isolated CH_4 molecule, which costs 103 kcal/mol (calculated at the DFT-BP+ZPE level of theory), the energy surface is thus very flat, which is due to the simultaneous formation of the OH bond with the breaking of the CH bond. When we go to free methyl radical and $(H_2O)_5Fe^{III}OH$, the net energy cost is only 14.4 kcal/mol with respect to the free reactants (16.5 kcal/mol with respect to the reactant complex). The 2.0 kcal/mol reaction energy needed to go from the reactant complex $Fe(IV)O\cdots HCH_3$ to the intermediate no. 2 $Fe(III)OH\cdots CH_3$ is still considerably smaller. The difference of 16.5−2.0 = 14.5 kcal/mol is the energy of the bond between the $CH_3^{\bullet}$ radical and the Fe(III)-OH complex, which is a three-center, two-electron bond, typically considerably stronger than a hydrogen bond but much weaker than a regular covalent bond. Also the 2+ charge on the complex has considerable effect, leading to an electrostatic component to the bond and to increased orbital interaction, cf. the substantial absolute increase of the charges *q*O and *q*CH_3 as the distance *R*(O−H) decreases and *R*(C−H) increases in Table 4, indicating the charge transfer from CH_3 to the iron complex; the charge on CH_3 becomes zero for the free radical formation. In the intermediate no. 2, the spin $S = 1/2$ of the methyl radical couples antiferromagnetically to the $S = 5/2$ of the $[(H_2O)_5Fe^{IV}OH]^{2+}$ complex to the same overall $S = 2$ we consistently have throughout these reactions.

For the second step in the oxygen-rebound mechanism, we find the formation of methanol bound to pentaaqua iron(II) to be very exothermic (46.6 kcal/mol), with again a very small barrier, equal to 3.1 kcal/mol. We did not succeed in finding this second transition state from geometry optimization along the unstable mode of the Hessian, due to convergence problems (which is a notorious problem of radicals bound weakly to transition metal complexes; e.g., see ref 27). However, from the potential energy surface (PES) shown in Figure 3, we could determine the transition-state structure to be the one shown in Figure 2. This two-dimensional potential energy surface was computed from a geometry optimization for each point (indicated by the crosses) constraining only the C−O bond distance and the H−O−C angle. The contour plot shows the PES in the plane through the O and H atoms of the hydroxo group and the C atom of methyl, with the oxygen situated at the origin (0,0), the q1 axis (q2 = 0) aligned through the O−H bond and the q2-axis thus perpendicular to the O−H bond. The energy of the $Fe^{III}-OH\cdots CH_3$ complex (i.e., intermediate no. 2), which is a local minimum on the energy surface, was set to zero in Figure 3. The potential energy surface shows that the intrinsic reaction coordinate is predominantly the H−O−C angle, i.e., the bound methyl radical can rotate around the hydroxo hydrogen to bind with the oxygen. The energy along the intrinsic reaction coordinate is very flat up to an H−O−C angle of about 60°, with a small maximum at an H−O−C angle of 30° (transition state no. 4), but then enters a very steep well associated with the irreversible formation of methanol. From the zero-Kelvin energy surface, this second step seems thus much more likely than dissociation of the $Fe(III)OH\cdots CH_3$

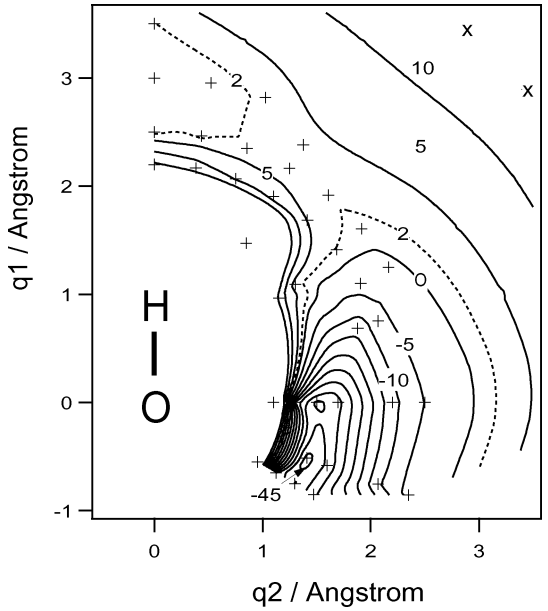

Figure 3. Contour diagram of the potential energy surface of the bound $^{\bullet}CH_3$ radical in the neighborhood of the hydroxo ligand, which were both produced in the first step of the oxygen-rebound mechanism. Each mark "+" indicates the carbon position of the methyl radical at which the energy was obtained from a geometry optimization of the complex, constraining only the C−O distance and the H−O−C angle. Oxygen is located at the point (0,0), and the R1 axis is chosen to lie on the O−H bond, as indicated. The R2 axis is perpendicular to it. With $^{\bullet}CH_3$ initially positioned close to (0,3), it can follow a bent channel with a small barrier of 3.1 kcal/mol toward the steep well at (1.4,−0.5), forming methanol bound to iron(II).

bond, i.e., formation of the free methyl radical. However, if we include zero-point energy effects, temperature corrections, and entropy effects, we see that the free energy barriers are similar, namely, 5.2 and 5.3 kcal/mol, respectively (see the numbers between parentheses in the panel for TS no. 4 and free Fe(III)-OH + CH_3 in Figure 2).

This rebound mechanism has also been theoretically predicted to be the reaction mechanism for the methane-to-methanol oxidation by the enzymes P450 and MMO (as aforementioned in the Introduction). In these complexes, an $Fe^{IV}O$ species is ligated by either a porphyrin ring via four nitrogens (P450) or octahedrally by none-heme ligands via connecting oxygens (MMO), which makes especially the latter interesting to compare our results with. Literature values for the energetics are compiled along with our results in Table 3. We see that also in these biological complexes the methane is initially very weakly bound in the reactant complex and that the overall formation of the product complex is very exothermic. The reaction barriers between, however, are significantly higher for the oxidation by the enzymes than by our water-ligated iron oxo species. For methane oxidation by P450, Ogliaro et al. found barriers of 26.7 kcal/mol for the hydroxylation and 29.1 kcal/mol for the rebound step, although the latter barrier vanishes if the system is allowed to cross to the low-spin surface.[35] Cytochrome P450 is known to be incapable of oxidizing methane, in contrast to MMO. Still, Basch et al. found a barrier for H-abstraction by MMO that is almost as high as the one for P450, equal to 23.2 kcal/mol.[29] Siegbahn found a much lower barrier with MMO, namely, 13.8 kcal/mol, which is still 11 kcal/mol higher than the barrier we find for the oxidation with aqua iron oxo.[27] Friesner et al. found the barrier to be 16 kcal/mol, a value between the results of Siegbahn and Basch et al.[33] The cited work on P450 and MMO was performed using the hybrid B3LYP functional, which is known to sometimes give better transition-state energies in cases where these barriers are underestimated by GGA functionals; for example, see ref 50. However, a comparison of these two functionals for the hydroxylation of H_2 by a bare iron oxo species showed that there is good agreement on the reaction barriers among the B3LYP and BP86 functionals, although the overall reaction exothermicity was found to be 10 kcal/mol smaller by the BP86 functional compared to the B3LYP functional.[18] Since discrepancies between the functionals are typically amplified in such small bare atom reactions, we expect much smaller discrepancies between energetics calculated with B3LYP and BP86 for the present complexes.

The O−H and C−H distances in transition state no. 3 (i.e., the one for the hydrogen abstraction step) (see Table 4) are very similar to those found for the biochemical analogues. For MMO, Siegbahn found $R_{OH} = 1.24$ Å and $R_{CH} = 1.30$ Å, and Basch et al. found $R_{OH} = 1.21$ Å and $R_{CH} = 1.33$ Å, which compares well with the values in our transition state ($R_{OH} = 1.20$ Å and $R_{CH} = 1.34$ Å). For the P450 transition state, Ogliaro et al. found $R_{OH} = 1.09$ Å and $R_{CH} = 1.50$ Å, which lies relatively closer to the $Fe^{III}-OH\cdots CH_3$ intermediate state. To summarize, we find that, apart from the higher barrier for hydroxylation in the MMO case, the rebound mechanism for methane-to-methanol oxidation by the pentaaqua iron(IV) oxo species is quite similar to the mechanism for the methane oxidation by MMO, calculated by Siegbahn. The hydrated ferryl ion in vacuo is found to be a highly reactive species, very well capable of hydroxylation and oxidation reactions with an organic substrate.

IV. Solvent Effects on H-Abstraction from Methane by Iron(IV) Oxo in Water

A. Car−Parrinello Molecular Dynamics Calculation of the Free Energy Barrier. The environment of a reacting system can have a strong influence on the thermodynamics of the reaction. This is why larger and larger parts of the bulky biological enzymes are taken into account in theoretical studies of the catalytically active centers of the enzymes, although solvent effects are usually still neglected. In this second part of the paper, we will examine the solvent effects on the energetics of the hydroxylation of methane by the ferryl ion in aqueous solution. An advantage of the methane oxidation by the ferryl ion is that the system is small enough to afford the inclusion of the traditional water solvent environment of the Fenton reaction in a Car−Parrinello molecular dynamics simulation. A disadvantage of methane is of course that it is not water soluble. We will return to this point in the discussion.

We have performed constrained molecular dynamics simulations to compute the free energy barrier, using the method of thermodynamic integration (e.g., see ref 51). Since in vacuo the reaction barrier for the methane hydroxylation was found to be much higher in the methane coordination mechanism (22.8 kcal/mol with respect to the reactant complex plus an additional 23.4 kcal/mol to create a vacant coordination site) than in the oxygen-rebound mechanism (3.5 kcal/mol), we have concentrated on the latter route in aqueous solution. The methane coordination mechanism in vacuo suffers, apart from the barrier with respect to the reactant complex, also from an additional endothermicity of 23.4 kcal/mol from the first step of H_2O/CH_4 ligand exchange. One could argue that this ligand exchange

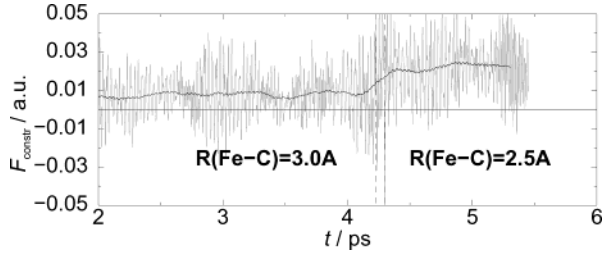

Figure 4. Force of constraint (gray line) and a running average (black line) during a constrained AIMD simulation of $[(H_2O)_4Fe^{IV}O(CH_4)]^{2+}$ in aqueous solution. Constraining the Fe−C bond length to 3.0 Å results in a repulsive force of 0.008 a.u. Moving the constraint to 2.5 Å (at $t \approx 4.25$ ps) increases the average to 0.022 au.

reaction energy would be much less endothermic in aqueous solution, due to the hydrophobic repulsion between the methane substrate and the solvent in contrast to the hydrophilic interaction between the water molecule and the solvent. In principle, computation of the ligand exchange reaction free energy in aqueous solution is possible, although cumbersome and a complicated reaction coordinate would be required. Instead, using a simple bond constraint, the interaction between the methane molecule and the iron site can be computed and compared to the −6 kcal/mol attraction at an Fe−C distance of $R_{FeC} = 3.0$ Å in vacuo. We therefore performed a short constrained molecular dynamics simulation of this system (e.g., see the reactant complex structure in Figure 1) in water, with the Fe−C bond distance constrained to 3.0 Å. The resulting average force of constraint is repulsive by 0.008 au, and similarly, an average force of constraint equal to 0.022 au is found for an Fe−C bond distance fixed at 2.5 Å (see Figure 4). The CH_4 molecule is thus repelled from the iron coordination site in aqueous solution, so we have concluded that the methane coordination mechanism does not offer a viable route in aqueous solution.

Proceeding with the oxygen-rebound mechanism, we performed nine subsequent constrained molecular dynamics simulations at different points along the reaction coordinate of the reaction

$$[(H_2O)_5Fe^{IV}O]^{2+} + CH_4 \rightarrow [(H_2O)_5Fe^{III}OH]^{2+} + {}^{\bullet}CH_3 \quad (6)$$

in water. The cubic supercell with an edge of 10.13 Å and subject to periodic boundary conditions contained one iron(IV) oxo molecule, one CH_4 molecule, and a total number of 31 H_2O molecules. The total 2+ charge was balanced by a uniformly distributed counter charge. A Nosé thermostat maintained a temperature of $T = 300$ K. The constrained reaction coordinate, ξ, was chosen to be a function of the O−H bond distance, R_{OH}, the C−O bond distance, R_{CO}, and the angle between these bonds, $\angle_{HOC}$:

$$\xi = 1 - \frac{R_{OH}\cos\angle_{HOC}}{R_{CO}} \quad (7)$$

The second term is the ratio of the projection of the O−H bond distance onto the C−O axis and the C−O bond distance, which equals $\xi = 0.5$ when the hydrogen is in the middle of the oxo ligand and the carbon. For infinitely separated reactants, ξ goes to 0, and for infinitely separated products, ξ goes to 1. Note that $\xi \geq 1$ for $\angle_{HOC} \geq 90°$, for instance when forming methanol, and second, $\xi < 0$ if $R_{OH} > R_{CO}$, for instance in freely rotating

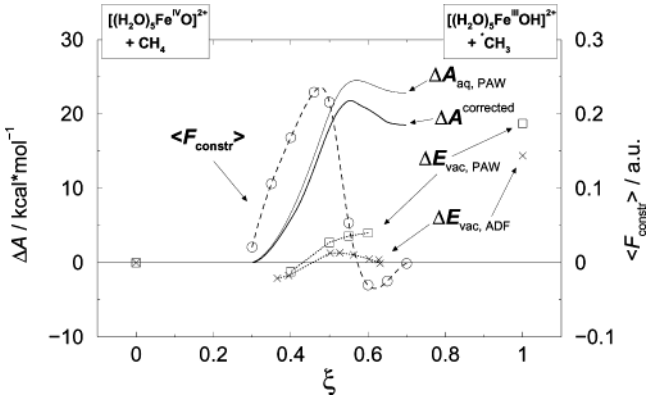

Figure 5. Helmholtz free energy profile ΔA (solid thin line) for methane hydroxylation by the ferryl ion in aqueous solution, obtained from the sampled mean forces of constraint (circles and dashed line; right-hand-side axis) of nine constrained AIMD runs. The discrepancy between the reaction energies of the hydroxylation in vacuo for the all-electron ADF calculation (crosses) and the approximate PAW calculation (squares) results in a correction to $\Delta A_{aq,PAW}$, the corrected ΔA_{aq} being given by the solid bold line (cf. text).

CH_4. For our nine MD simulations, we choose $\xi = (0.30, 0.35, 0.40, 0.45, 0.50, 0.54, 0.60, 0.65, 0.70)$. Each simulation started by bringing the constrained reaction coordinate ξ to the desired value during a short MD run, after which an equilibration MD run followed by at least 2.5 ps to adapt the system to the new constraint value until there was no longer any drift in the fluctuating force of constraint. We then sampled the force of constraint, λ_ξ, during a 2 ps MD simulation. To correct λ_ξ for the bias introduced by imposing the constraint, which limits the sampling to a constrained NVT ensemble, instead of the desired true NVT ensemble, the true force of constraint $F(\xi)$ was calculated using

$$F(\xi) = \frac{\langle \lambda_\xi Z^{-1/2}\rangle_\xi + \frac{1}{2}k_B T\left\langle Z_\xi^{-5/2}\sum_{i=1}^{N}\frac{1}{m_i}\nabla_i\xi\cdot\nabla_i Z\right\rangle_\xi}{\langle Z^{-1/2}\rangle_\xi}$$

$$Z = \sum_i \frac{1}{m_i}\left(\frac{\partial\xi}{\partial \mathbf{r_i}}\right)^2 \quad (8)$$

where T is the temperature, k_B is Boltzmann's constant, m_i and $\mathbf{r_i}$ are the mass and the position of atom i, and λ_ξ is the sampled Lagrange multiplier associated with the holonomic constraint $\xi - \xi'(r) = 0$.[52]

The results, the forces of constraint for nine points along the reaction coordinate, are shown in Figure 5, indicated by the open circles (and the right-hand-side axis) and fitted with a quadratic spline (dashed line). Due to the limited size of the supercell, the reaction coordinate value of $\xi = 0.3$ is practically the largest possible separation of the reactants in the box. The average distance between the oxo ligand and the methane carbon equals $R_{CO} = 3.44$ Å at this constraint value (see Figure 6, for the relevant average interatomic distances, R_{CO}, R_{OH}, R_{CH}, and R_{FeO} as a function of the reaction coordinate ξ). The average distance between the methane carbon and its hydrogen (that is to be transferred to the oxo ligand) is $R_{CH} = 1.114$ Å at $\xi = 0.3$, which is almost equal to the other three average C−H bond distances (1.107 Å). The interaction between the reactants at $\xi = 0.3$ is indeed very small, but not completely zero, as seen

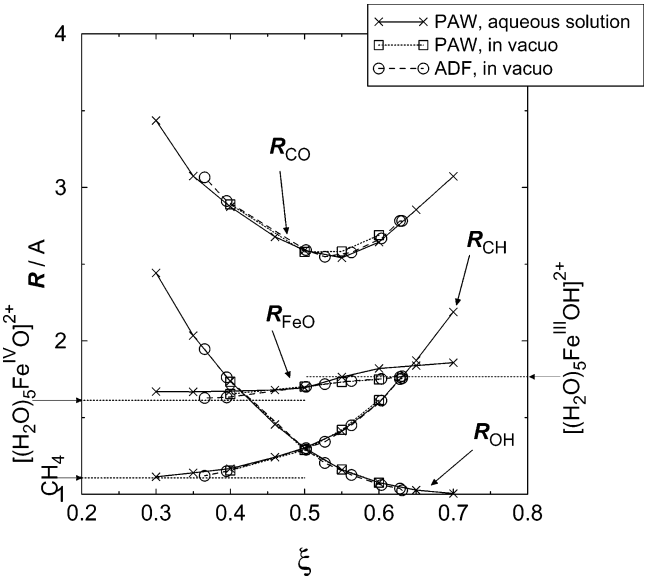

Figure 6. Most relevant bond distances as a function of the reaction coordinate ξ. The bond distances in vacuo and the (average) distances in solution are very similar, except for R_{FeO}. In vacuo, the Fe−O distance for $[(H_2O)_5Fe^{IV}O]^{2+}$ ($\xi = 1$) is reached rapidly, as indicated by the horizontal dotted line, and similarly the Fe−O distance for $[(H_2O)_5Fe^{III}OH]^{2+}$ ($\xi = 0$) at the other end. In aqueous solution, the average Fe−O bond length is always significantly larger.

from the small value for the mean force of constraint at $\xi = 0.3$ in Figure 5. Moving along the reaction coordinate to larger ξ results initially in an increasing repulsive force, which comes to a maximum at $\xi = 0.477$ and then decreases again to cross the zero mean force of constraint at $\xi = 0.580$, which marks the transition state. Initially, the reactants are just pulled toward each other, as shown by the rapid decrease in the averages of R_{CO} and R_{OH} (see Figure 6). But beyond $\xi = 0.4$, also R_{CH} is seen to increase rapidly, indicating the transfer of the hydrogen from methane to the oxo ligand. The average distance between the oxo ligand and the methane carbon, R_{CO}, has its minimum at the transition-state position of $\xi = 0.580$.

The Helmholtz free energy profile is obtained by integrating the mean force of constraint with respect to ξ:

$$A(\xi) = \int F(\xi) d\xi + C \tag{9}$$

The result is shown by the thin solid line in Figure 5 (connected to the left-hand-side axis). We choose C such that the free energy equals zero for our point with the lowest ξ value, $\xi = 0.3$. The bold solid line shows the modified free energy profile, ΔA_{aq}, for the hydrogen abstraction from methane by the ferryl ion in water, after correcting for the discrepancy between results for the reaction energy of the hydrated complexes in vacuo obtained with the accurate all-electron ADF computation and with the approximate PAW approach, as explained in the Method Section. We have also plotted these reaction energies of the hydrated complexes in vacuo in Figure 5 for comparison, using dotted lines and squares (labeled $\Delta E_{vac,ADF}$) and crosses (labeled $\Delta E_{vac,PAW}$). The reaction free energy barrier of 21.8 kcal/mol (with respect to the reactant complex at $\xi = 0.3$) is much higher than the zero-Kelvin energy barrier found for the H-abstraction in vacuo of 3.4 kcal/mol. Inclusion of the temperature-dependent internal energy, $\Delta E_{int}^{300K} = -4.8$ kcal/mol, and the entropy contribution, $-T\Delta S = 2.5$ kcal/mol (see Table 3), to this latter number, results in a free energy barrier of 1.1 kcal/mol in vacuo, making the difference in energetics even larger (the zero-point energy is not included in the computed Helmholtz free energy of the reaction in solution and is therefore also omitted in this number for the reaction in vacuo). The large difference between the free energy profile in aqueous solution and the reaction energy in vacuo is notable, but it is well-known that for a charged system large effects may occur. Moving further to the product side, ΔA_{aq} slowly decreases again by 3.3 kcal/mol, to 18.5 kcal/mol with respect to the reactant state at $\xi = 0.3$.

B. Analysis of Solvent Effects. Although the method of constrained molecular dynamics is in principle an exact method to compute free energy differences for a system in solution,[51,52] statistical errors are introduced due to the limited length of the trajectories. In a previous work, we estimated this error for the free energy barrier of the S_N2 reaction between Cl^- and CH_3Cl to be 3 kcal/mol.[50] However, we found the S_N2 reaction in water to be a worst case scenario because during the course of the reaction, as the charge moves from the attacking Cl^- to the leaving Cl^-, the attacking Cl^- loses four water molecules from its coordination shell, while at the same time the leaving Cl^- builds up a coordination shell. This slow process requires extremely long simulation times, which led in this case to a free energy barrier that was 3 kcal/mol too high. 3 kcal/mol should thus be regarded as an upper limit for the error.

The reaction free energy barrier for hydrogen abstraction from methane by the ferryl ion is 20 kcal/mol higher in aqueous solution than it is in vacuo. One of our concerns was that the difference could be attributed to an erroneous electronic spin state of the product iron(III)hydroxo complex in aqueous solution. That is, with the excess number of up-spin electrons fixed to four with respect to the number of down-spin electrons, giving a total spin of $S = 2$, the iron(III)hydroxo complex can either be in the $S = 5/2$ high-spin state, antiferromagnetically coupled to the $S = -1/2$ $^{\bullet}CH_3$ radical, or in the $S = 3/2$ low-spin state coupled to a parallel $S = 1/2$ $^{\bullet}CH_3$ radical. For example, regarding the $[(H_2O)_5Fe(III)OH\cdots{}^{\bullet}CH_3]^{2+}$ complex in vacuo, we found an energy difference of 11.5 kcal/mol between this complex with iron(III) in the $S = 5/2$ high-spin ground state and that with iron(III) in the energetically higher $S = 3/2$ spin state (in both cases, the electron spin on $^{\bullet}CH_3$ coupled antiparallel to that on the iron complex). To verify the spin-state on iron(III) in solution, we computed the electron spin density (i.e., the difference between the up-spin and down-spin total electron densities) of snapshots from the constrained MD simulations of the product state. Figure 7 shows the spin density (isosurfaces of 0.02 e) of a molecular configuration at a constrained reaction coordinate value of $\xi = 0.7$. As expected, the spin density is located on the $^{\bullet}CH_3$ radical, the iron ion, and to a lesser extent, the water and hydroxo ligands. The negative (blue) density on $^{\bullet}CH_3$ and the positive (yellow) density on the iron complex indeed shows the antiferromagnetic coupling between the products, which confirms that the iron complex has the expected $S = 5/2$ high-spin state.

Having established that the increased reaction barrier in solution is not due to a change in the electronic spin state, the solvent environment apparently has a strong effect on the

(51) Frenkel, D.; Smit, B. *Understanding Molecular Simulation*, Academic: San Diego, CA, 1996.
(52) den Otter, W. K.; Briels, W. J. *J. Chem. Phys.* **1998**, *109*, 4139.

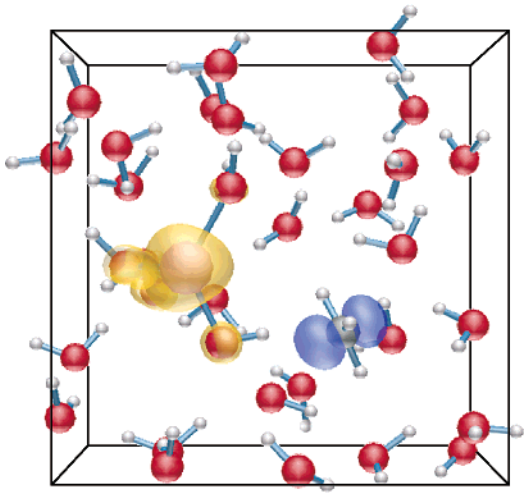

Figure 7. Electron spin density and ball−stick representation of a constrained molecular dynamics snapshot of the unit cell containing the $^{\bullet}CH_3$ radical and iron(III)hydroxo complex products in aqueous solution at a reaction coordinate value $\xi = 0.7$. The spin density, mainly localized on the products, is negative (blue) on $^{\bullet}CH_3$ and positive (yellow) on the iron(III) complex, confirming the antiferromagnetic coupling between the $^{\bullet}CH_3$ $S = 1/2$ spin state with the iron(III) $S = 5/2$ spin state.

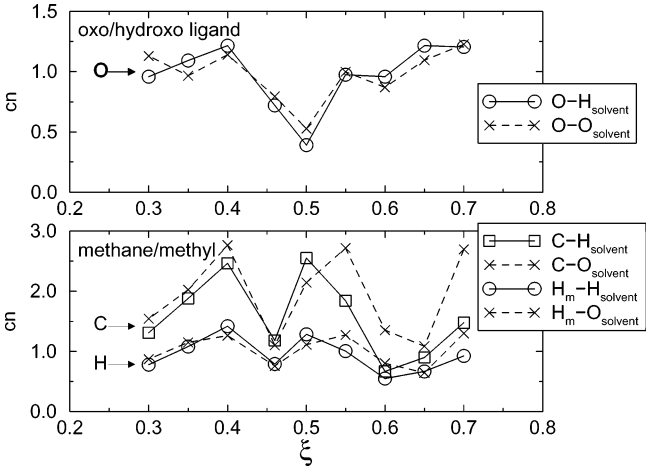

Figure 8. Solvation of the reacting species during the hydroxylation in water measured by the coordination numbers of the oxo/hydroxo ligand oxygen (upper graph) and of the methane/methyl-radical carbon and hydrogens (lower graph). Circles, squares, and solid lines show the average number of solvent hydrogens with a certain radius around the atom, and crosses and dashed lines show the number of oxygens with a certain radius around the atom.

energetics of the abstraction reaction, which is not completely unexpected for a charged reaction complex. The hydration of the iron complex and the methyl by the surrounding dipolar water molecules plays an important role, as the charge distribution over the reactants changes along the reaction coordinate, leading to changes in the solvation energy. We are not able to quantitatively calculate the solvation energy with its long-range (dielectric response) contribution; however, we can analyze the changes in the short-range solvent structure during the reaction, which will make the largest contribution to the change in solvation energy. Since the charge on the complex remains the same, the long-range contribution is expected to change little. We have therefore expressed the hydration of the oxo atom and the carbon and its (three) hydrogens in solvent coordination numbers, *cn*, by integrating the radial distribution functions of these atoms with respect to the solvent hydrogens and solvent oxygens up to certain radii. For the oxo/hydroxo ligand oxygen, the radial distributions, $g_{OHs}(r)$ and $g_{OOs}(r)$, showed clear peaks due to the hydration by, on average, one water molecule, and the upper integration limit was therefore chosen at the minimum after the peaks at $r_{OHs} = 2.25$ Å and $r_{OOs} = 3.00$ Å. For the methane/methyl carbon and hydrogens, the hydrophobic solvation does not result in sharp peaks in the radial distribution functions, so that here the integration limits were chosen judiciously to be $r_{CHs} = 3.0$ Å, $r_{COs} = 3.5$ Å, $r_{HmHs} = 2.5$ Å, and $r_{HmOs} = 3.0$ Å (the subscript s meaning solvent and m meaning methyl). Figure 8 shows these solvent coordination numbers for the oxo/hydroxo ligand (upper graph) and the methane/methyl substrate (lower graph).

The hydration of the hydrogen abstracting oxygen shows a clear picture: at the reactant side, the oxo ligand is coordinated by on average one water molecule, and at the product side, the hydroxo ligand also accepts on average one (1.2) hydrogen bond from a solvent molecule. In between, the hydration decreases to a minimum of about 0.4 hydrogen bonded solvent molecule at $\xi = 0.5$. This decrease is partly explained by the approaching methane, which disrupts the solvent structure around the oxo-ligand as the distance between the oxygen and the methane carbon, R_{CO} (Figure 6), decreases. However, the oxo coordination is not so small at $\xi = 0.55$ and 0.60 even though R_{CO} is still small. Most likely, the increased charge transfer (polarization) in the transition-state complex relative to the reactant complex that we observed for the hydrated complexes in vacuo (see Table 4) also takes place during the hydrogen transfer in solution. As a result, the oxygen becomes more negative in the transition-state configuration (at $\xi = 0.58$ in aqueous solution) and therefore more attractive for H-bond-donating solvent molecules, hence the increased coordination number at $\xi = 0.55$ and 0.60, compared to $\xi = 0.50$.

The coordination number of the carbon (and methyl hydrogens) initially increases, as the methane molecule becomes polarized when one C−H becomes slightly elongated (lower graph in Figure 8). But again cn drops when the distance between methane and the oxo ligand, R_{CO}, decreases, and part of the solvation shell of methane has to make space for the oxo ligand to enter. Also here, the minimum in cn is again followed by a significant increase, which must be due to the increased (now positive) charge on CH_3, which we also noticed in vacuo (Table 4).

Although we have discussed in detail the effects of H-bonding changes of oxo and methyl, this does not establish conclusively the origin of the increase of the barrier. We cannot exclude other possible effects: changes in coordination of first and second coordination shell waters and dielectric response effects. What conclusions can we draw from these studies of the effect of water solvent for the viability of the ferryl ion as a reaction intermediate in oxidation reactions by Fenton's reagent? The reaction free energy barrier of more than 20 kcal/mol for the rate-determining step (i.e., the H-abstraction) in the oxidation of methane in aqueous solution, is on the high side. However, as explained in the Introduction, the reaction barrier for methane hydroxylation serves as an upper limit. The C−H bond energy in a more typical organic substrate such as tartaric acid (as was used by H. J. H. Fenton himself[1,2]) is on the order of 10 kcal/mol less than that in methane. The remaining 10 kcal/mol for the barrier of the hydroxylation is not high at all, so this result in combination with our previous work on the ferryl ion

formation from Fenton's reagent leads us to conclude that the ferryl ion is indeed a likely candidate for the active species in Fenton chemistry. A definitive answer will have to come from simulations in water solution using a water-soluble typical organic substrate for the Fenton oxidation. In addition, we note that it may be interesting to consider other solvents, notably ones that can be expected to have smaller screening effects. Such solvents can be expected to lower the barrier for the H-abstraction considerably compared to water, to the point that even methane oxidation might become feasible.

V. Conclusion

We have performed static DFT calculations and ab initio (DFT) molecular dynamics simulations to study the ability of the ferryl ion $[Fe^{IV}O]^{2+}$ to oxidize organic substrates in aqueous solution. In the first part of this work, we have shown with static DFT calculations that the hydrated ferryl ion $[(H_2O)_5Fe^{IV}O]^{2+}$ is indeed very reactive and can oxidize methane to methanol in vacuo. We have tested and compared two reaction mechanisms that have been proposed for the methane-to-methanol oxidation by the bare ferryl ion on one hand and by the ferryl ions that form the active cores of certain biological enzymes on the other. In the second part of this work, we have studied the role of the reactants' environment by taking into account the full aqueous solvent environment in the ab initio molecular dynamics approach.

Via the so-called methane coordination mechanism, with one water ligand replaced by methane, the weakly interacting reaction complex first forms a iron(IV)−hydroxo-methyl complex by hydrogen transfer from the methane to the oxo ligand. Then, methanol is formed in a second exothermic step by transfer of the CH_3 group from the metal to the hydroxo oxygen. The first step is the rate-limiting step with a barrier of 22.8 kcal/mol. The energetics for the methane coordination mechanism in our water-ligated iron complex are quite different from those of the methane oxidation by bare metal oxo species, for which this mechanism was found to be the most likely one. The water−methane ligand exchange reaction preceding the actual H-abstraction is endothermic by 23.4 kcal/mol.

Via the alternative mechanism, the so-called oxygen-rebound mechanism, the methane-to-methanol oxidation, is practically barrierless in vacuo and also proceeds in two steps. First, a hydrogen is abstracted from methane by the oxo ligand, forming an $[Fe^{III}OH\cdots{}^{\bullet}CH_3]^{2+}$ complex. Then, the bound $^{\bullet}CH_3$ radical can transfer via a narrow channel to the hydroxo oxygen, again forming methanol. Overall, this mechanism shows strong similarities with methane oxidation by the enzyme methane monooxygenase and, to a lesser extent, with oxidation by cytochrome P450, although the calculated barriers in the cases of these biocatalysts are significantly higher.

Solvent effects are important when dealing with charged reactants. We have therefore studied the solvent effects on the initial methane hydroxylation step in the oxygen-rebound mechanism in aqueous solution. The free energy barrier of the H-abstraction from methane in aqueous solution is estimated to be 22 kcal/mol, using the method of constrained molecular dynamics. The reaction barrier and the overall endothermicity of this first step are thus significantly higher in solution than they are in vacuo, which is related to the decreased hydration of the reacting oxo/hydroxo ligand in the transition state and the higher energy of solvation for the iron(IV) oxo ion compared to the iron(III) hydroxo ion. These findings cannot be generalized immediately to more typical organic substrates in the Fenton oxidation, which are water-soluble and typically have weaker C−H bonds (ca. 10 kcal/mol). The barrier might therefore be ca. 10 kcal/mol lower, which would make the oxidation with the ferryl ion as an active intermediate a perfectly viable route. Actual simulations with larger organic substrates, to quantify the solvent effects, will have to provide definitive verification.

In combination with our previous work on Fenton's reagent (a mixture of iron(II) ions and hydrogen peroxide in water), which showed the spontaneous formation of the much contested ferryl ion, this work supports the mechanism proposed by Bray and Gorin for the oxidation of organic substrates by Fenton's reagent, with the ferryl ion as the active species.

Acknowledgment. We gratefully acknowledge the support by the Prioriteits Programma Materialen—Computational Materials Science (PPM-CMS). We thank the foundation NCF of The Netherlands Foundation of Scientific Research (NWO) for computer time.

JA038865A